

## Catalysts

Glucose- and Cellulose-Derived Ni/C-SO<sub>3</sub>H Catalysts for Liquid Phase Phenol HydrodeoxygenationStanislav Kasakov,<sup>[a]</sup> Chen Zhao,<sup>[a, b]</sup> Eszter Baráth,<sup>[a]</sup> Zizwe A. Chase,<sup>[c]</sup> John L. Fulton,<sup>[d]</sup> Donald M. Camaioni,<sup>[d]</sup> Aleksei Vjunov,<sup>[d]</sup> Hui Shi,<sup>[d]</sup> and Johannes A. Lercher\*<sup>[a, d]</sup>

**Abstract:** Sulfonated carbons were explored as functionalized supports for Ni nanoparticles to hydrodeoxygenate (HDO) phenol. Both hexadecane and water were used as solvents. The dual-functional Ni catalysts supported on sulfonated carbon (Ni/C-SO<sub>3</sub>H) showed high rates for phenol hydrodeoxygenation in liquid hexadecane, but not in water. Glucose and cellulose were precursors to the carbon supports. Changes in the carbons resulting from sulfonation of the carbons resulted in variations of carbon sheet structures, morphologies and the surface concentrations of acid sites. While the C-SO<sub>3</sub>H supports were active for cyclohexanol dehydration in hexadecane and water, Ni/C-SO<sub>3</sub>H only catalysed the reduction of phenol to cyclohexanol in water. The state of 3–5 nm grafted Ni particles was analysed by in situ

X-ray absorption spectroscopy. The results show that the metallic Ni was rapidly formed in situ without detectable leaching to the aqueous phase, suggesting that just the acid functions on Ni/C-SO<sub>3</sub>H are inhibited in the presence of water. Using in situ IR spectroscopy, it was shown that even in hexadecane, phenol HDO is limited by the dehydration step. Thus, phenol HDO catalysis was further improved by physically admixing C-SO<sub>3</sub>H with the Ni/C-SO<sub>3</sub>H catalyst to balance the two catalytic functions. The minimum addition of 7 wt% C-SO<sub>3</sub>H to the most active of the Ni/C-SO<sub>3</sub>H catalysts enabled nearly quantitative conversion of phenol and the highest selectivity (90%) towards cyclohexane in 6 h, at temperatures as low as 473 K, suggesting that the proximity to Ni limits the acid properties of the support.

## Introduction

Effective utilization of biomass as a renewable source of energy and feedstock for conversion to useful chemicals hinges upon designing highly active and stable catalysts.<sup>[1,2]</sup> A one-step efficient conversion of lignin-derived phenolic oil, such as lignin waste from industrial paper production,<sup>[3–5]</sup> has yet to be developed. This approach requires multifunctional catalysts that have sufficient contact with reactants and high stability of the active sites under process conditions.

To achieve this, we have prepared and studied a series of dual-functional catalysts that are able to hydrodeoxygenate

phenols.<sup>[6–13]</sup> These catalysts include physical mixtures of noble metals and mineral acids (Pd supported on active carbons (Pd/C) and aqueous phosphoric acid),<sup>[6,7]</sup> base metals and solid acids (Raney Ni and Nafion<sup>®</sup>),<sup>[8]</sup> as well as those integrating metal-acid bifunctionality in one catalyst particle (Pd/HZSM-5, Pd/HBEA and Ni/HZSM-5).<sup>[9–14]</sup> Base-metal catalysts such as Ni, Co, and Fe supported on carbon are less frequently investigated,<sup>[15,16]</sup> because it is challenging to incorporate nanosized particles of these metals onto the carbon supports.<sup>[17–19]</sup>

Suitable carbon materials can be produced by pyrolysis of biogenic sources. The chemical composition, morphology, specific surface area, and functional group density of such carbon materials is influenced by the carbon precursor, the synthesis procedure including physical or chemical activation as well as post-synthetic treatments.<sup>[20–24]</sup> Such subsequent treatments on carbon materials derived from carbohydrates result, for example, in acid sites on the outer surface of carbon sheets (e.g., C-SO<sub>3</sub>H or C-COOH, etc.), which are known to be catalytically active for several acid-catalysed reactions.<sup>[25–28]</sup> Cellulose and glucose were chosen as carbon precursors in this work, because both are the main components of woody biomass, so minimizing the carbon footprint of the catalyst.

The synthetic anchoring of Ni particles onto sulfonated carbon is challenging, because of the thermal instability of carbon supports and especially of C-SO<sub>3</sub>H groups in air and N<sub>2</sub> at high temperatures, making conventional calcination and reduction treatments of Ni salts unfeasible. Therefore, grafting of metallic Ni nanoparticles, produced by reduction of Ni salt pre-

[a] S. Kasakov, Dr. C. Zhao, Dr. E. Baráth, Prof. Dr. J. A. Lercher  
Department of Chemistry and Catalysis Research Center  
Technische Universität München, Garching 85747 (Germany)  
E-mail: johannes.lercher@ch.tum.de

[b] Dr. C. Zhao  
Current address: Shanghai Key Laboratory of Green Chemistry and  
Chemical Process, Department of Chemistry, East China Normal University  
North Zhongshan Road 3663, 200062 Shanghai (P.R. China)

[c] Z. A. Chase  
School of Chemical and Biological Engineering  
Washington State University, Pullman, WA 99364 (USA)

[d] Dr. J. L. Fulton, Dr. D. M. Camaioni, A. Vjunov, Dr. H. Shi,  
Prof. Dr. J. A. Lercher  
Institute for Integrated Catalysis, Pacific Northwest National Laboratory  
902 Battelle Boulevard, Richland WA 99352 (USA)

Supporting information for this article is available on the WWW under  
<http://dx.doi.org/10.1002/chem.201405242>.

cursors by borane triethylamine, was used.<sup>[29]</sup> This technique does not require high-temperature treatment, and leads to well-permitted dispersed Ni nanoparticles with accessible surface acid sites on the carbon supports.

In this contribution, we report a novel dual-functional Ni/C-SO<sub>3</sub>H catalyst that exhibits remarkably high activity towards phenol hydrodeoxygenation (HDO) in liquid hexadecane at mild reaction conditions (473 K, 4 MPa H<sub>2</sub>). An in-depth ex situ and in situ characterization of sulfonated carbon supports, and Ni-incorporated carbon catalysts permitted the correlation of catalyst properties and catalytic activity. Mutual influences of metal and acid sites anchored either on one (Ni/C-SO<sub>3</sub>H) or physically mixed (C-SO<sub>3</sub>H + Ni/C-SO<sub>3</sub>H) carbon sheets were investigated with respect to the model reaction of phenol HDO.

## Results and Discussion

### Synthesis, characterization, and activity tests of carbon catalysts

Glucose and cellulose were selected for the synthesis of carbons. Both were pyrolyzed in N<sub>2</sub> atmosphere at 673 K for 15 h yielding carbon black, labelled as C<sub>Gl</sub> and C<sub>Ce</sub>, respectively. Carbonization of ZnCl<sub>2</sub>/HCl-impregnated glucose or cellulose precursors in N<sub>2</sub> resulted in the formation of high-surface (HS) carbons, identified as C<sub>Zn-Gl</sub> and C<sub>Zn-Ce</sub>, respectively. These four carbon materials were subsequently functionalized with sulfonic acid sites (–SO<sub>3</sub>H) by treatment with concentrated sulfuric acid (96 wt %) at 423 K in flowing N<sub>2</sub>.

### Textural property and acidity of synthesized carbon materials

The physiochemical properties of carbon materials, that is, specific surface areas, pore volumes, and acid site distributions are compiled in Table 1. The N<sub>2</sub> sorption analysis shows that the specific BET surface areas of the carbon black materials C<sub>Gl</sub> and C<sub>Ce</sub> were quite small (< 25 m<sup>2</sup> g<sup>−1</sup>). However, in the presence of ZnCl<sub>2</sub> the specific surface areas increased 70- and 30-fold (1388 and 793 m<sup>2</sup> g<sup>−1</sup>) for C<sub>Zn-Gl</sub> and C<sub>Zn-Ce</sub>, respectively. The N<sub>2</sub> sorption data indicate that parent C<sub>Gl</sub> and C<sub>Ce</sub>, with pore volumes of 0.07 and 0.08 cm<sup>3</sup> g<sup>−1</sup>, respectively, were nonporous materials (isotherm and hysteresis shown in the Supporting Information, Figure S1). The HS carbons had two- to three-times higher pore volumes than carbon black, that is, 0.14 and 0.22 cm<sup>3</sup> g<sup>−1</sup> from glucose and cellulose precursors, respectively. Zinc chloride is a moderate Lewis acid, which disrupts structural features of the precursor leading to carbon materials with higher specific surface areas and pore volumes.<sup>[30]</sup> Due to their non-porous textures, the impact of the sulfuric acid treatment on the specific surface areas of carbon blacks was minimal, whereas the surface areas of the HS carbons C<sub>Zn-Gl</sub> and C<sub>Zn-Ce</sub> decreased by 20% to 1189 and 622 m<sup>2</sup> g<sup>−1</sup>, respectively. Remarkably, sulfonation increased the pore volumes of the four carbon materials by two- to fourfold, to 0.14–0.19 and 0.39–0.50 cm<sup>3</sup> g<sup>−1</sup> for the sulfonated carbon black and HS carbons, respectively. It is speculated that sulfonation minimizes the

**Table 1.** Physiochemical properties of LS and HS carbons as well as their sulfonated counterparts.

Sample	S <sub>BET</sub> [m <sup>2</sup> g <sup>−1</sup> ]	V <sub>micropore</sub> [cm <sup>3</sup> g <sup>−1</sup> ]	Acidity [mmol g <sup>−1</sup> ] <sup>[a]</sup>		
			–SO <sub>3</sub> H	–COOH	–OH
C <sub>Gl</sub>	< 20	0.07	–	–	–
C <sub>Zn-Gl</sub>	1388	0.14	–	–	–
C <sub>Ce</sub>	25	0.08	–	–	–
C <sub>Zn-Ce</sub>	793	0.22	–	–	–
C <sub>Gl</sub> -SO <sub>3</sub> H	< 20	0.14	0.85	0.35	0.11
C <sub>Zn-Gl</sub> -SO <sub>3</sub> H	1189	0.50	0.90	0.55	0.40
C <sub>Ce</sub> -SO <sub>3</sub> H	24	0.19	1.00	0.25	0.20
C <sub>Zn-Ce</sub> -SO <sub>3</sub> H	622	0.39	1.10	0.40	0.35

[a] Analysed by Boehm titration.

carbon structure leading to smaller surface areas, the strong acidic environment breaking down the carbon sheets, which results in larger micropore volumes in the carbon structures.

The treatment with sulfuric acid in N<sub>2</sub> atmosphere produces acid functional groups, that is, –SO<sub>3</sub>H, –COOH, and aromatic –OH groups on the external surface of the layered or stacked carbon sheets. Boehm titration was applied to determine the concentration surface acid sites in the final carbon materials. For all, the concentration of surface acidic groups increased in the sequence –SO<sub>3</sub>H > –COOH > aromatic–OH (Table 1). Additional treatment with ZnCl<sub>2</sub>/HCl increased the total concentration of acid sites of –SO<sub>3</sub>H, –COOH, and aromatic–OH by 0.05–0.10, 0.15–0.20, and 0.15–0.19 mmol g<sup>−1</sup>, respectively. However, it was also observed that the differences in surface area between the glucose and cellulose precursors as well as carbon black and HS carbons did not lead to considerable differences in the concentration of sulfonic groups. Thus, very similar –SO<sub>3</sub>H acid site concentrations (0.85–1.10 mmol g<sup>−1</sup>) were determined for the four sulfonated carbon samples.

### Morphology of the carbon and sulfonated carbon materials

The incorporation of ZnCl<sub>2</sub>/HCl into glucose and cellulose precursors led to enhancement of surface areas and pore volumes of carbon materials (Table 1). The variations in their morphologies are evident in the SEM images (Figure 1 and Figure S2 in the Supporting Information). The C<sub>Zn-Gl</sub> material retained the rigid triangular shape with an average particle size of approximately 100 μm (Figure 1a), whereas the sulfonated material had a highly disordered foam-like structure with increased concentrations of defects as well as with a reduction of rigid structures (Figure 1b). These observations are in accordance with the significant increase of pore volume of C<sub>Zn-Gl</sub> from 0.14 to 0.50 cm<sup>3</sup> g<sup>−1</sup> after ZnCl<sub>2</sub>/HCl treatment (Table 1). In comparison, the C<sub>Zn-Ce</sub> and C<sub>Zn-Ce</sub>-SO<sub>3</sub>H materials were similar, the SEM images of both exhibiting soft graphene-like sheets in a fibrous network (Figure 1c and d).

SEM images of glucose-derived C<sub>Gl</sub> and cellulose-derived C<sub>Ce</sub> carbons and their sulfonated counterparts are displayed in Figure S2 in the Supporting Information. The C<sub>Gl</sub> carbon black showed a rigid flake-shape texture (Figure S2a), whereas the

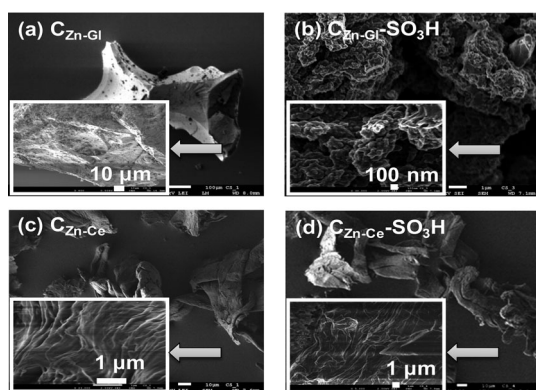


**Figure 1.** SEM images of HS carbons and corresponding sulfonated counterparts. a) HS carbon from pyrolyzed glucose with  $\text{ZnCl}_2$ , and b) sulfonated as-synthesized HS carbon from glucose, c) HS carbon from pyrolyzed cellulose, and d) sulfonated HS carbon from cellulose with  $\text{ZnCl}_2$ .

$\text{C}_{\text{Ce}}$  carbon black appeared as a fibrous strip without a distinct structure (Figure S2c). Upon sulfonation, the morphology of  $\text{C}_{\text{Gl}}\text{-SO}_3\text{H}$  was almost unchanged (Figure 1 b), while  $\text{C}_{\text{Ce}}\text{-SO}_3\text{H}$  showed more pronounced fibrous carbon strips with a smoothing of the surface (Figure S2d), demonstrating a highly disordered amorphous structure.

### Carbon framework structures and surface $\text{-SO}_3\text{H}$ functional groups of HS carbons

The major carbon species in the sulfonated HS carbon were speciated by  $^{13}\text{C}$  MAS solid NMR spectroscopy (Figure 2a). The chemical shifts at 130, 150 and 180 ppm in the NMR spectrum are assigned to polycyclic aromatic carbon atoms, phenolic hydroxyl, and carboxylic groups, respectively.<sup>[31]</sup> While aromatic carbons attached to  $\text{-SO}_3\text{H}$  groups would appear at 140 ppm, this shift region is overlapped by broad bands assigned to aromatic carbon atoms at 130 ppm and aromatic carbons attached to hydroxyl groups at 150 ppm. Based on  $^{13}\text{C}$  solid-state NMR data, the carbon framework components of HS carbon from glucose and cellulose (before and after sulfonation) are very similar. The  $\text{ZnCl}_2/\text{HCl}$  aided carbonization of cellulose and glucose (HS carbons) resulted primarily in polycyclic aromatic groups with the framework structures of graphene sheets. The introduction of sulfonic acid groups converted these surface sheets partly to amorphous  $\text{sp}^3$  hybridized carbon.

The concentrations of surface  $\text{SO}_3\text{H}$  groups attached to the carbon materials were measured by energy dispersive X-ray analysis (EDX; Figure 2b). The results show that the concentration of surface  $\text{-SO}_3\text{H}$  groups were  $0.80 \text{ mmol g}^{-1}$  for  $\text{C}_{\text{Zn-Gl}}\text{-SO}_3\text{H}$  and  $1.05 \text{ mmol g}^{-1}$  for  $\text{C}_{\text{Zn-Ce}}\text{-SO}_3\text{H}$ , agreeing well with the Boehm titration results, that is, 0.90 and  $1.10 \text{ mmol g}^{-1}$ , respectively (Table 1). TGA-MS measurements ( $\text{SO}_2$  fragment,  $m/e$  64, Figure 2c) show that the  $\text{C-SO}_3\text{H}$  group started to decompose at 620 K for cellulose-derived  $\text{C}_{\text{Zn-Ce}}\text{-SO}_3\text{H}$  catalyst, while it occurred at 710 K for glucose-derived  $\text{C}_{\text{Zn-Gl}}\text{-SO}_3\text{H}$ . This implies that glucose-derived carbons have a higher thermal

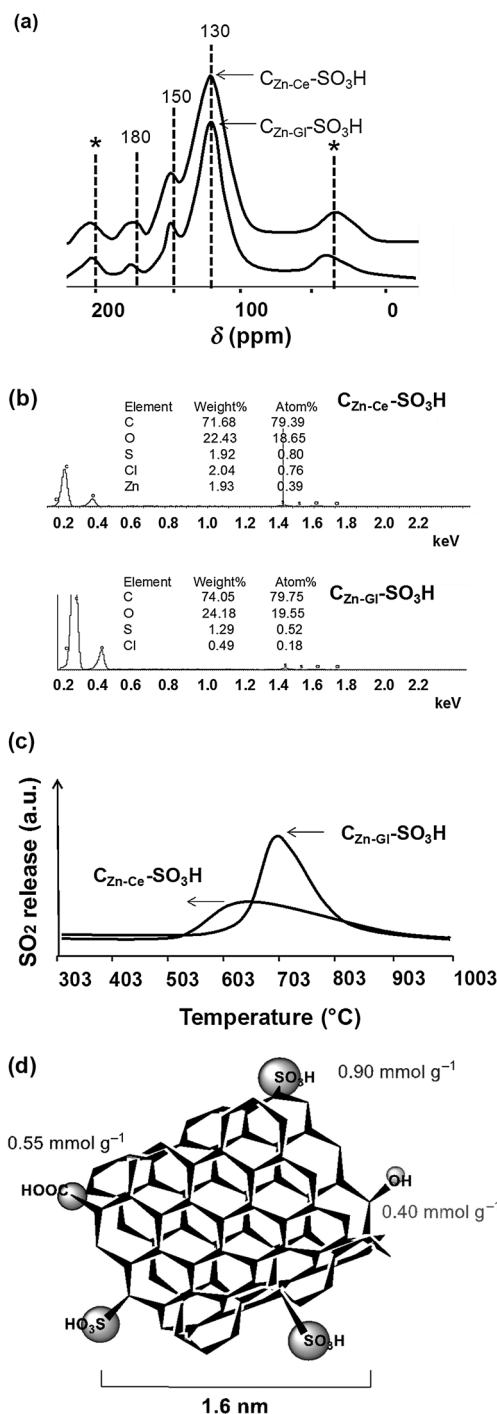


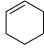
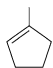
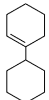
**Figure 2.** a)  $^{13}\text{C}$  MAS solid-state NMR spectrum, b) EDX spectra, c) TGA-MS of two sulfonated HS carbons, and d) proposed structure of the functionalized carbon sheet of glucose-derived HS carbon ( $\text{C}_{\text{Zn-Gl}}\text{-SO}_3\text{H}$ ).

stability of  $\text{C-SO}_3\text{H}$  bonds attached to the carbon sheet surface. The proposed structure of the functionalized carbon sheets of HS carbon is depicted in Figure 2d. The acid functional groups of  $\text{-SO}_3\text{H}$ ,  $\text{-COOH}$ , and  $\text{-OH}$  are concluded to be anchored on the edges of carbon sheets with a graphene domain size of 1.6 nm, determined by Raman spectroscopy<sup>[32]</sup> and described in the Supporting Information in detail (Figures S3 and S4).

## Correlation of activities of cyclohexanol dehydration with structural properties of C-SO<sub>3</sub>H materials

The acidic properties of the sulfonated carbons were evaluated with respect to the dehydration of cyclohexanol (a key step in phenol HDO) in hexadecane (Table 2). The selected materials encompass the four sulfonated carbons described in this work, as well as three commercial carbons after sulfonation. Cyclohexene was the major product, with selectivities above 96% in all cases. Other olefinic products were isomerized 1-methyl-cyclopentene and condensed 1-cyclohexyl-cyclohexene. Parent carbons did not convert cyclohexanol showing that the active sites are related to the surface sulfonate groups.<sup>[25,26]</sup> Acidic sites (–COOH and –OH) of lower strength are less abundant (Table 1) and are concluded to be less active than sulfonate groups. The initial turnover frequencies (TOFs) for dehydration were 120–498 mol mol<sup>–1</sup><sub>[SO<sub>3</sub>H]</sub> h<sup>–1</sup> over C-SO<sub>3</sub>H (Table 2, entries 1–3).

**Table 2.** Dehydration of cyclohexanol using sulfonated carbon catalysts.<sup>[a]</sup>

Entry	Catalyst	Conv. [%]	Selectivity [C%]			Rate <sup>[b]</sup> [mmol g <sup>–1</sup> h <sup>–1</sup> ]	TOF <sup>[b]</sup> [mol mol <sup>–1</sup> <sub>[SO<sub>3</sub>H]</sub> h <sup>–1</sup> ]
							
1	C-SO <sub>3</sub> H <sup>[c]</sup>	58	96	2.0	1.5	120	341
2	C-SO <sub>3</sub> H <sup>[d]</sup>	29	97	2.0	0.2	30	120
3	C-SO <sub>3</sub> H <sup>[e]</sup>	68	98	1.5	0.2	150	498
4	C <sub>GI</sub> -SO <sub>3</sub> H	59	96	1.0	1.0	130	153
5	C <sub>Zn-GI</sub> -SO <sub>3</sub> H	100	98	1.0	1.0	260	289
6	C <sub>CE</sub> -SO <sub>3</sub> H	48	97	2.0	0.2	80	80
7	C <sub>Zn-CE</sub> -SO <sub>3</sub> H	100	98	1.7	1.0	170	153

[a] Reaction conditions: cyclohexanol (10 g), catalyst (0.5 g), hexadecane (80 mL), 4.0 MPa H<sub>2</sub> (ambient temperature), 473 K, 1 h, stirring at 700 rpm. [b] The initial rates and TOFs were determined at reaction conditions: cyclohexanol (20 g), catalyst (0.1 g), hexadecane (80 mL), 4.0 MPa H<sub>2</sub> (ambient temperature), 473 K, 1 h, stirring at 700 rpm, see Supporting Information Table S2. [c] Carbon source: active carbon Darco®, acid-washed lignite carbon, granular. [d] Carbon source: active charcoal Norit® W35, from peat, steam activated. [e] Carbon source: active charcoal DARCO® KB-G.

Interestingly, commercial carbon materials which were treated with acid during the carbonization procedure (entries 1 and 3) showed low surface sulfonate concentration but a much higher concentration of carboxylic acid sites (Table S2 in the Supporting Information). The sulfonated commercial carbon materials show apparently high activities per surface sulfonate group. This, however, led overall to a slightly lower activity per mass of the catalyst (30–150 mmol g<sup>–1</sup> h<sup>–1</sup>) than the home-made carbon samples prepared in this work (Table 2). In addition, these commercial active carbons are usually produced by pyrolysis at high temperature, above 1023 K, which leads to sp<sup>2</sup> cross-linking of the polycyclic aromatic carbon sheets that may have limited access of the reactant molecules.<sup>[33,34]</sup>

Reactions with glucose and cellulose derived C<sub>GI</sub>-SO<sub>3</sub>H and C<sub>CE</sub>-SO<sub>3</sub>H yielded 59 and 48% olefins from cyclohexanol, with dehydration rates of 130 and 80 mmol g<sup>–1</sup> h<sup>–1</sup>, respectively (Table 2). Normalized to the surface –SO<sub>3</sub>H concentrations, the corresponding TOFs were 153 and 80 mol mol<sup>–1</sup><sub>[SO<sub>3</sub>H]</sub> h<sup>–1</sup>. Reac-

tions with the sulfonated HS carbons led to quantitative cyclohexanol dehydration under identical conditions, reaching rates as high as 289 and 153 mmol g<sup>–1</sup> h<sup>–1</sup>, respectively. Since the –SO<sub>3</sub>H concentrations are almost identical between the sulfonated low-surface (LS) and HS samples (Table 1), the higher TOFs (289 and 153 mol mol<sup>–1</sup><sub>[SO<sub>3</sub>H]</sub> h<sup>–1</sup> for HS glucose and cellulose derived carbon) are attributed to increased accessibility of the acid sites (Table 1).

## Characterization and activity evaluation of Ni/C-SO<sub>3</sub>H catalyst

### Ex situ analysis of Ni/C-SO<sub>3</sub>H catalysts

The physicochemical properties of four sulfonated carbon supports are compiled in Table 3 incorporated with Ni nanoparticles, prepared by liquid-phase Ni(acac)<sub>2</sub> reduction with Et<sub>3</sub>N-BH<sub>3</sub> protected by oleylamine and oleic acid surfactants. (Comparison of catalysts prepared by other methods is de-

tailed in the Supporting Information, Table S4.) The Ni contents were determined by ICP-OES to be 9.2, 9.4, 9.7, and 9.9 wt% for Ni/C<sub>GI</sub>-SO<sub>3</sub>H, Ni/C<sub>Zn-GI</sub>-SO<sub>3</sub>H, Ni/C<sub>CE</sub>-SO<sub>3</sub>H, and Ni/C<sub>Zn-CE</sub>-SO<sub>3</sub>H catalysts, respectively. The total acidities of the four catalysts were measured by the Boehm-titration method giving overall Brønsted acidity, which varies between 1.55 and 1.85 mmol g<sup>–1</sup>. Note that the amount of the accessible –SO<sub>3</sub>H sites was actually decreased by about 10% after the Ni incorporation, as one Ni atom with the oxidation state 2+ consumes 2OH<sup>–</sup>, and therefore increases the consumption of HCl as titrant. All catalysts show lower specific surface

areas and pore volumes after Ni incorporation (Tables 1 and 3). The Ni catalysts supported on sulfonated LS carbon (C<sub>GI</sub>-SO<sub>3</sub>H and C<sub>CE</sub>-SO<sub>3</sub>H) had two orders of magnitude lower surface areas than those supported on HS carbons. With respect to the HS carbons, the BET surface area of the Ni/C<sub>Zn-CE</sub>-SO<sub>3</sub>H decreased by one order of magnitude (622 vs. 68 m<sup>2</sup> g<sup>–1</sup>), while the surface area of C<sub>Zn-GI</sub>-SO<sub>3</sub>H decreased by half upon Ni incorporation (1189 vs. 613 m<sup>2</sup> g<sup>–1</sup>). After Ni incorporation, the pore volumes of sulfonated carbon black were almost filled up by the newly formed Ni nanoparticles, that is, decreased to non-measurable values for Ni/C<sub>GI</sub>-SO<sub>3</sub>H and Ni/C<sub>CE</sub>-SO<sub>3</sub>H (vs. 0.14 and 0.19 cm<sup>3</sup> g<sup>–1</sup> for C<sub>GI</sub>-SO<sub>3</sub>H and C<sub>CE</sub>-SO<sub>3</sub>H, respectively). For the HS carbons, the pore volume of C<sub>Zn-CE</sub>-SO<sub>3</sub>H decreased from 0.39 to 0.08 cm<sup>3</sup> g<sup>–1</sup> after Ni loading, whereas the pore volume of Ni/C<sub>Zn-GI</sub>-SO<sub>3</sub>H was almost unchanged (0.54 vs. 0.50 cm<sup>3</sup> g<sup>–1</sup>), probably due to the special pore structure and rigid morphology of the HS samples as discussed on detailed in the previous section.



**Table 3.** Physicochemical properties and Ni particle sizes of Ni/C-SO<sub>3</sub>H catalysts.

Catalyst	Ni content [wt%] <sup>[a]</sup>	Total acidity [mmol g <sup>-1</sup> ] <sup>[b]</sup>	S <sub>BET</sub> [m <sup>2</sup> g <sup>-1</sup> ]	V <sub>volume</sub> [cm <sup>3</sup> g <sup>-1</sup> ]	d <sub>TEM</sub> [nm] <sup>[c]</sup>
Ni/C <sub>Gl</sub> -SO <sub>3</sub> H	9.2	1.55	< 20	0.06	5.3 ± 2.3
Ni/C <sub>Zn-Gl</sub> -SO <sub>3</sub> H	9.4	1.79	613	0.54	3.8 ± 1.1
Ni/C <sub>Ce</sub> -SO <sub>3</sub> H	9.7	1.68	< 20	0.01	4.2 ± 1.2
Ni/C <sub>Zn-Ce</sub> -SO <sub>3</sub> H	9.9	1.85	68.0	0.08	3.5 ± 0.8

[a] Determined by ICP-OES; [b] determined by Boehm titration; [c] determined by TEM images (300 Ni particles were counted for estimating particle sizes).

The representative TEM images of the Ni particles grafted on the four sulfonated carbon supports are shown in Figure 3, along with the particle-size distributions obtained from statistical analysis of at least 300 Ni particles from the TEM images. Ni nanoparticles on cellulose-derived carbon black (Ni/C<sub>Ce</sub>-SO<sub>3</sub>H) exhibited an average size of 4.3(±1.3) nm. Larger and less uniform particles (5.3(±2.3) nm) were observed for Ni/C<sub>Gl</sub>-SO<sub>3</sub>H. When deposited on the sulfonated HS carbon (Ni/C<sub>Zn-Ce</sub>-SO<sub>3</sub>H and Ni/C<sub>Zn-Gl</sub>-SO<sub>3</sub>H), the Ni nanoparticles decreased in average size (3.8 and 3.5 nm) with a slight smaller deviation (1.1 and 0.8 nm). These results suggest that surface structure and morphology of the carbon support influence the size and distribution of supported Ni particles after the addition of the common batch of presynthesized Ni particles.

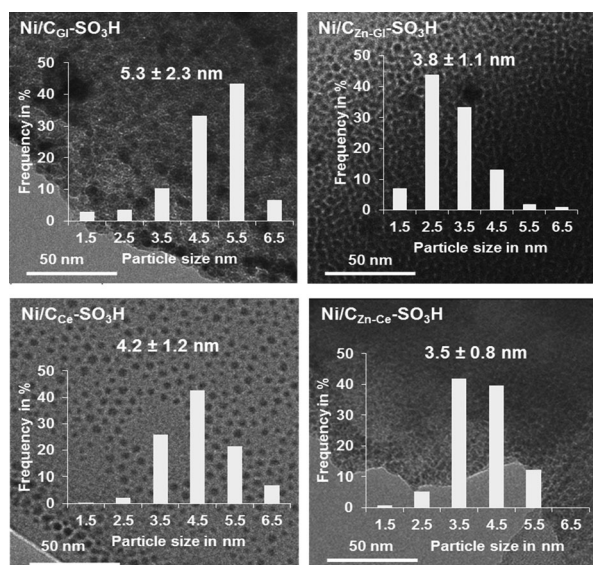


**Figure 3.** TEM images and particle size distribution diagrams of Ni nanoparticles grafted on the four sulfonated carbon supports.

### In situ spectroscopic study of Ni state during aqueous phase phenol hydrodeoxygenation

The impact of the condensed phase (H<sub>2</sub>O, hexadecane) on the reducibility of the metal as well as the catalyst stability under reaction conditions was explored by in situ X-ray absorption spectroscopy (XAS). The state of Ni and its particle size in the

Ni/C<sub>Zn-Gl</sub>-SO<sub>3</sub>H catalyst were investigated by XAS during phenol HDO. Figure 4 contains the near-edge (XANES) portion of the spectra of the 10 wt% Ni/C<sub>Zn-Gl</sub>-SO<sub>3</sub>H during HDO of 0.56 M phenol/water solution at 473 K and a total pressure of 5 MPa. To determine the concentration of both the Ni<sup>0</sup> and Ni<sup>II</sup> phase as a function of time, we simulated the XANES spectra as linear combinations of Ni foil (473 K), NiO and α-Ni(OH)<sub>2</sub> standards.

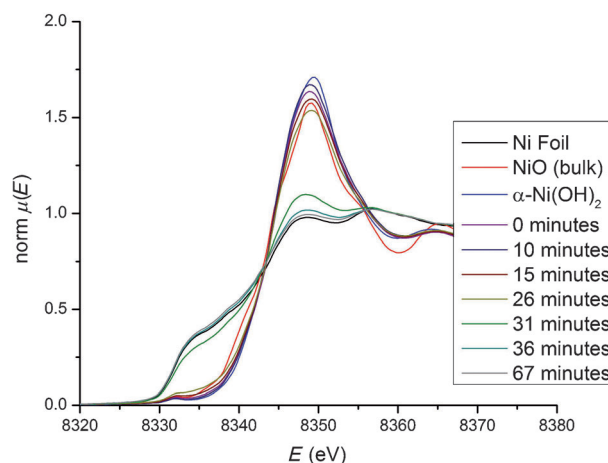


**Figure 4.** Changes in the oxidation state of Ni in 10 wt% Ni/C<sub>Zn-Gl</sub>-SO<sub>3</sub>H monitored by the white line intensity in XANES at different time intervals during phenol hydrogenation (0.56 M aqueous solution) at 473 K and a total pressure (mainly H<sub>2</sub> and water vapour) of approximately 5 MPa. The black curve represents the Ni foil standard, the red curve represents the nanoparticle NiO standard, and the blue curve is the nanoparticle α-Ni(OH)<sub>2</sub> standard.

Figure 5 shows the fractions of the Ni<sup>0</sup> and Ni<sup>II</sup> species in the catalysts as a function of time during the aqueous phase HDO of phenol. Initially, the Ni particles were 100% in the Ni<sup>II</sup> state, or specifically, a 20:80 mixture of NiO and Ni(OH)<sub>2</sub>. The reduction to Ni<sup>0</sup> started after 12 min, that is, when the temperature of 473 K was reached, and proceeded to completion within 50 min. The metallic state of Ni dominated after 30 min following the start of the reaction. During the experiment, a phenol conversion of 33% was attained in 67 min, corresponding to a TOF of 180 mol<sub>phenol</sub> mol<sub>Ni</sub><sup>-1</sup> h<sup>-1</sup>. This value represents a lower boundary condition as the concentration of Ni<sup>0</sup> increased during the kinetic measurements.

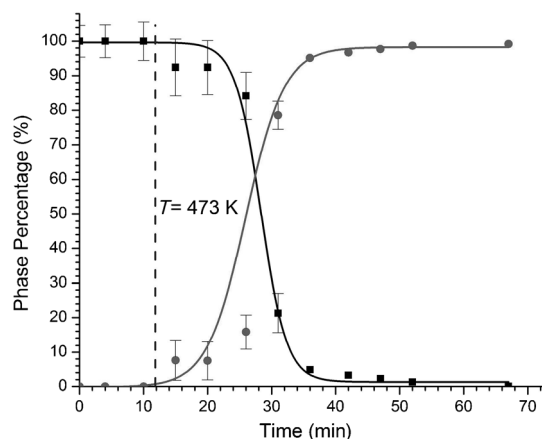
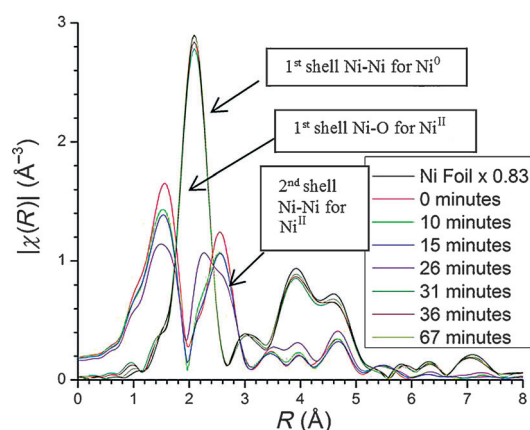
The spectra of Ni K-edge for 10 wt% Ni/C<sub>Zn-Gl</sub>-SO<sub>3</sub>H measured prior to (ex situ) and at the end of reduction in H<sub>2</sub> are shown at Figures S5 and S6 in the Supporting Information, respectively. Table 4 provides values for the first shell coordination numbers for the Ni nanoparticles. The Ni coordination numbers upon complete reduction were above 10, corresponding to an average particle size greater than 4.5 nm.<sup>[36]</sup> The structural disorder and first shell Ni–Ni bond length after 70 min of reaction match that of the Ni metal standard.

Also, the amplitude of the sample at 67 min (Figure 6) closely matches that of bulk Ni, suggesting that Ni particles have a bulk-like structure. The concentration of Ni in the beam did not change, indicating that leaching did not occur under hy-

**Table 4.** The first shell Ni–O and second shell Ni–Ni nearest-neighbour geometries of the Ni nanoparticles at the start and the end of the HDO reaction with 10 wt % Ni/C<sub>Zn-Gl</sub>-SO<sub>3</sub>H after 67 min (*k*-weight of 2).<sup>[a]</sup>

State	Length [Å]		CN		Debye–Waller factor, $\sigma^2 \times 10^{-3}$ [Å <sup>2</sup> ]	
	Ni–O	Ni–Ni	Ni–O	Ni–Ni	Ni–O	Ni–Ni
Ni <sup>0</sup> (ex situ)	2.071 (12)	2.989 (7)	6	12	7.9 (11)	9.1 (13)
Ni <sup>0</sup> (473 K, 67 min)	N/A	2.498 (4)	N/A	10.4 (3)	N/A	9.8 (1)
NiO bulk (298 K)	2.076 (16)	2.956 (11)	6	12	7.0 (15)	6.3 (5)
Ni Foil (473 K)	N/A	2.499 (4)	N/A	12	N/A	9.4 (1)

[a] Errors shown in the parentheses refer to the error to the last significant digit. N/A = not applicable.

**Figure 5.** Changes in the composition of the Ni nanoparticles (10 wt % Ni/C<sub>Zn-Gl</sub>-SO<sub>3</sub>H) during phenol hydrogenation (0.56 M aqueous solution) at 473 K and a total pressure (mainly H<sub>2</sub> and water vapour) of approximately 5 MPa. The black curve shows the percentage of the Ni<sup>0</sup> phases during reaction. The grey curve represents the percentage of the metallic Ni phase. The reactor reached 473 K in 12 min (dashed line) and right after the reaction temperature was reached the phase change began.**Figure 6.** The Ni K-edge spectra of the  $\chi(R)$  magnitude of Ni foil (black line) to that of 10 wt % Ni/C-SO<sub>3</sub>H as a function of time at 473 K and 5 MPa  $P_{H_2}$ .

drothermal conditions. Song et al. also observed that Ni nanoparticles grafted on HBEA did not leach in apolar solvents using Soxhlet extraction at 353 K and 1 bar air.<sup>[37]</sup>

## Phenol reduction on Ni/C-SO<sub>3</sub>H in aqueous phase

All catalysts were active in hydrogenation of phenol with high selectivities (95–97 %) for cyclohexanol (Table S5 in the Supporting Information). Nickel supported on C<sub>Zn-Gl</sub>-SO<sub>3</sub>H was the most active. However, cyclohexene or cyclohexane were not observed. As is shown by EXAFS, water

does not negatively impact the state of Ni<sup>0</sup>; Ni was rapidly reduced under the reaction conditions and stayed in the catalyst without leaching.

The absence of alkenes and alkanes in the products clearly indicates that the acid sites in the Ni/C-SO<sub>3</sub>H catalysts are not able to catalyse alcohol dehydration. Since the Ni was nearly 100 % in the metallic state after the induction period, the acid exchange sites should be free from Ni<sup>2+</sup>. In the absence of Ni, C-SO<sub>3</sub>H catalysed the dehydration of cyclohexanol in water (Table S3 in the Supporting Information). At this point, we speculate that the acid sites were rendered inactive, neutralized by adventitious poisons (e.g., residual bases from the incorporation of Ni) or exchanged by Ni<sup>2+</sup> such that protons were hardly present. Importantly, by switching to a non-polar solvent, hexadecane, the acid site was able to catalyse the dehydration of cyclohexanol (Table 5) and the cascade reactions of phenol HDO.

## Evaluation of phenol hydrodeoxygenation catalysed by Ni/C-SO<sub>3</sub>H in the non-polar liquid phase (hexadecane)

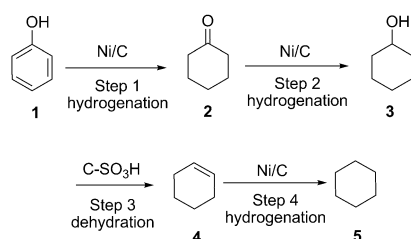
The four Ni/C-SO<sub>3</sub>H catalysts were tested for phenol HDO in hexadecane solvent at 473 K and 4 MPa H<sub>2</sub> (Table 5). Scheme 1 shows the sequential reactions for phenol HDO in the liquid phase over dual functional metal/acid sites.<sup>[6–11]</sup> The steps involve sequential hydrogenation of phenol to cyclohexanol over Ni sites, dehydration of cyclohexanol over the acidic C-SO<sub>3</sub>H sites, and cyclohexene hydrogenation over the Ni sites to cyclohexane. The catalysts based on glucose-derived carbon materials showed higher HDO activity than those based on cellulose-derived carbons (entries 1–4). The C<sub>Ce</sub>-SO<sub>3</sub>H and C<sub>Zn-Ce</sub>-SO<sub>3</sub>H supported Ni catalysts delivered 75–80 % conversion, while phenol conversion reached 95–100 % on C<sub>Gl</sub>-SO<sub>3</sub>H and C<sub>Zn-Gl</sub>-SO<sub>3</sub>H supported catalysts. As the Ni particle sizes of these catalysts were similar, the higher HDO activity seems to be related to the carbon morphologies and pore structures, which permit greater interaction of phenol with Ni. In addition, it is also observed that the use of HS carbon slightly enhanced HDO activity for Ni/C-SO<sub>3</sub>H (Table 5). This modest increase, however, does not seem directly proportional to the differences in surface areas and pore volumes of the carbon materials (Table 1).

All four products (2–5) in Scheme 1 were detected. Cyclohexanol was the major product (50–60 % selectivity), while cyclohexanone was formed only in trace amounts (< 5 % selectivity).

**Table 5.** Hydrodeoxygenation of phenol with Ni/C-SO<sub>3</sub>H catalysts.<sup>[a]</sup>

Entry	Catalyst	Conv. [%]	Selectivity [C %]			
			—one	—ol	—ene	—ane
1	Ni/C <sub>Gl</sub> -SO <sub>3</sub> H	95	4	55	18	20
2	Ni/C <sub>Zn-Gl</sub> -SO <sub>3</sub> H	100	5	50	15	25
3	Ni/C <sub>Ce</sub> -SO <sub>3</sub> H	75	4	65	9	20
4	Ni/C <sub>Zn-Ce</sub> -SO <sub>3</sub> H	82	2	59	13	23
5	physically mixed C <sub>Zn-Gl</sub> -SO <sub>3</sub> H + Ni/C <sub>Zn-Gl</sub> -SO <sub>3</sub> H (0.1 g g <sup>-1</sup> )	98	1	18	25	55
6	C <sub>Zn-Gl</sub> -SO <sub>3</sub> H + Ni/C <sub>Zn-Gl</sub> -SO <sub>3</sub> H (0.2 g g <sup>-1</sup> )	64	4	50	12	29
7	C <sub>Zn-Gl</sub> -SO <sub>3</sub> H + Ni/C <sub>Zn-Gl</sub> -SO <sub>3</sub> H (0.5 g g <sup>-1</sup> )	38	9	69	5	12

[a] Reaction conditions: phenol (0.60 g), Ni/C-SO<sub>3</sub>H (0.12 g), C-SO<sub>3</sub>H (0.06, 0.024, 0.012 g), hexadecane (60 mL), 473 K, 4 MPa H<sub>2</sub>, stirring at 700 rpm, 2 h.

**Scheme 1.** Reaction sequences on hydrodeoxygenation of phenol in the liquid phase.

ity). This is consistent with observations that Ni catalyses the hydrogenation of cyclohexanone at much higher rates than of phenol.<sup>[12]</sup> The presence of a substantial concentrations of cyclohexene (9–18%) suggests that the Ni-catalysed cyclohexene hydrogenation rate was significantly lower than with noble metals such as Pd or Pt.<sup>[6,7]</sup>

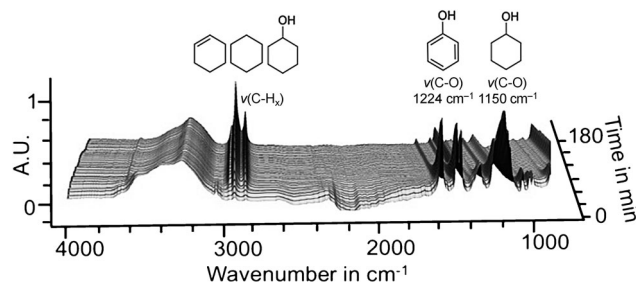
The selectivity to HDO products (alkane and alkene) was lower than 50% on all Ni/C-SO<sub>3</sub>H catalysts at 473 K. As the formation of these products depends on cyclohexanol dehydration, the temperature was raised from 453 to 523 K in the hope that increasing the rate of cyclohexanol dehydration would increase the yield. These results are depicted in Figure S7 in the Supporting Information. It shows that raising the temperature from 453 to 523 K increased the conversion of phenol from 80 to 100% under otherwise identical conditions, but the selectivity to alkane/alkene products remained at about 30%. Cyclohexanol was still the major product with approximately 60% selectivity, while cyclohexanone was produced with a selectivity lower than 5%. This means that phenol HDO in hexadecane on the Ni/C-SO<sub>3</sub>H catalysts is limited by the dehydration of cyclohexanol over a significant temperature range. To test this hypothesis, in situ IR experiments were performed and analysed further.

#### In situ IR spectroscopy of the reaction pathway of phenol HDO catalysed by Ni/C-SO<sub>3</sub>H in liquid hexadecane

As shown in Figure 7, the compounds can be identified by their characteristic vibration modes, that is, the aromatic C–O

stretch vibration in the case of phenol the aliphatic C–O stretch vibration for cyclohexanol as intermediate. The C–H stretching vibrations are associated with cyclohexanone, cyclohexanol, cyclohexene, as well as cyclohexane. The carbonyl group in cyclohexanone, which has an IR band at 1700 cm<sup>-1</sup> was not detected, due to its relatively low concentration (3–5% selectivity).

Although the extinction coefficients for the IR bands are not

**Figure 7.** Time-resolved in situ IR spectroscopy study during phenol HDO over Ni/C<sub>Zn-Gl</sub>-SO<sub>3</sub>H in hexadecane as solvent at 473 K and 3 MPa H<sub>2</sub>.

known, the time-resolved IR spectra (Figure 8) provide semi-quantitative information on the kinetics. With increasing reaction time, the intensity of IR peaks of phenol (1224 cm<sup>-1</sup> aromatic CO stretch) declined, while cyclohexanol (1067 cm<sup>-1</sup> aliphatic CO stretch) increased first and then slowly dropped to a low value, indicating that cyclohexanol was still present after 180 min of reaction. The sharp increase of the C–H<sub>x</sub> stretching vibration peaks (2928 cm<sup>-1</sup> representing the CH<sub>x</sub> peaks) demonstrates the high hydrogenation rates on the nanosized Ni particles. Thus, the rate-determining step is shown to be the dehydration of cyclohexanol.

#### Optimization of phenol HDO catalysis by Ni/C-SO<sub>3</sub>H in liquid hexadecane

Based on the insight from in situ IR studies, we attempted to accelerate the rates of cyclohexanol dehydration, the limiting step in phenol HDO in hexadecane, by adding sulfonated carbon (C<sub>Zn-Gl</sub>-SO<sub>3</sub>H) with the supported Ni/C<sub>Zn-Gl</sub>-SO<sub>3</sub>H catalyst (Table 5, entries 5–7). Interestingly, the additional amounts of sulfonated carbon influenced not only the dehydration of cyclohexanol but also the hydrogenation of phenol. A mixture of 0.012 g C<sub>Zn-Gl</sub>-SO<sub>3</sub>H and 0.12 g Ni/C<sub>Zn-Gl</sub>-SO<sub>3</sub>H catalyst produced an almost quantitative conversion of phenol (98%) with a high selectivity to cyclohexene and cyclohexane (combined 80 C%). Mixtures with higher ratios (0.2–0.5 g g<sup>-1</sup>) of the C<sub>Zn-Gl</sub>-SO<sub>3</sub>H showed only lower rates of phenol conversion. A 0.07 g g<sup>-1</sup> or 1:15 ratio by weight was determined to be optimum. The re-

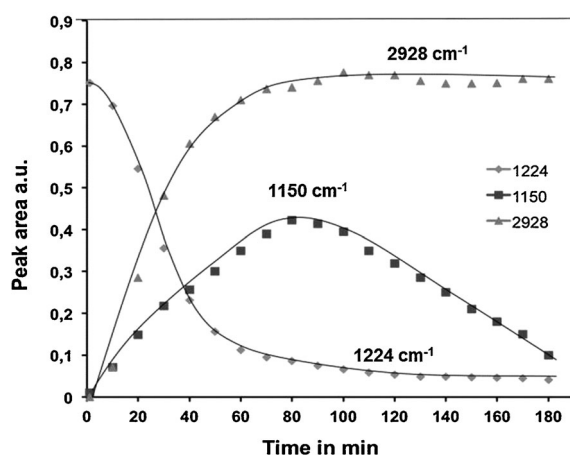


**Figure 8.** Relative trend of the phenol hydrogenation ( $1224\text{ cm}^{-1}$ ) to cyclohexanol ( $1067\text{ cm}^{-1}$ ) as intermediate and the cumulative  $\text{CH}_x$  ( $2928\text{ cm}^{-1}$ ) formation.

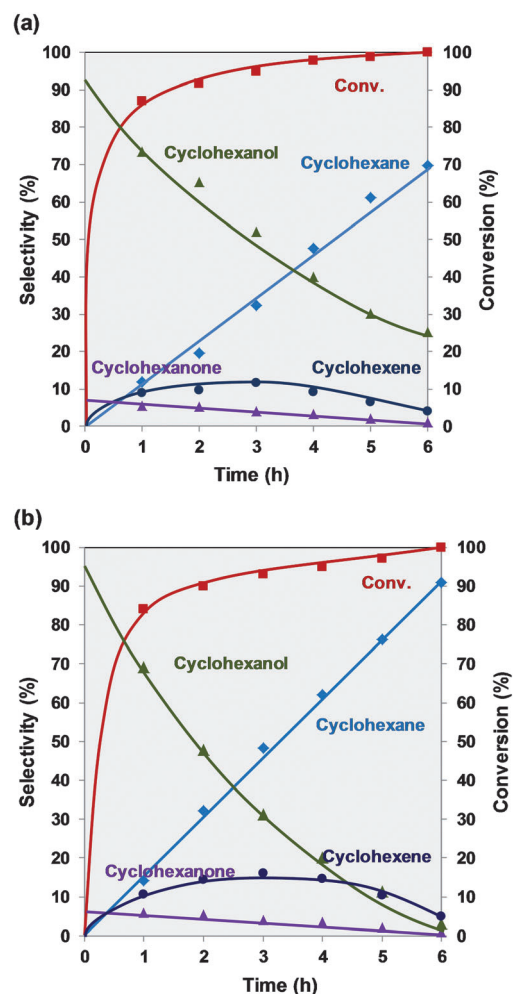
sults suggest that the sulfonic acid groups interact with Ni directly or indirectly, reducing its availability for hydrogenation.

Figure 9 compares the HDO of phenol in hexadecane at 473 K in the presence of 4 MPa  $\text{H}_2$  over the  $\text{Ni/C}_{\text{Zn-GI}}\text{-SO}_3\text{H}$  catalyst and over the optimum 1:15 (wt/wt) mixture of  $\text{C}_{\text{Zn-GI}}\text{-SO}_3\text{H}$  and  $\text{Ni/C}_{\text{Zn-GI}}\text{-SO}_3\text{H}$ . The initial products on  $\text{Ni/C}_{\text{Zn-GI}}\text{-SO}_3\text{H}$  were cyclohexanol (92% selectivity) and cyclohexanone (8% selectivity). Subsequently, dehydration of cyclohexanol produced cyclohexene. Cyclohexene was further hydrogenated to cyclohexane, becoming the major product at longer times (70% yield at 6 h). For the optimized mixture of  $\text{C}_{\text{Zn-GI}}\text{-SO}_3\text{H}$  and  $\text{Ni/C}_{\text{Zn-GI}}\text{-SO}_3\text{H}$ , hydrogenation of phenol and cyclohexene were found to be relatively unaffected by the added  $\text{C}_{\text{Zn-GI}}\text{-SO}_3\text{H}$  material, but the dehydration rates increased, as indicated by the faster conversion of cyclohexanol. Whereas  $\text{Ni/C}_{\text{Zn-GI}}\text{-SO}_3\text{H}$  produced 75% cyclohexane/ene after 6 h, the optimum mixture achieved 95% cyclohexane/ene formation in 6 h under the same conditions. The conversion was maintained above 90% on  $\text{Ni/C}_{\text{Zn-GI}}\text{-SO}_3\text{H}$  after three runs, showing high stability of both Ni and acid sites attached to the carbon sheets during phenol HDO in hexadecane.

## Conclusion

Bifunctional, highly active, and stable catalysts have been developed that combine metallic Ni nanoparticles (3–5 nm) with acidic sulfonated HS carbons derived from glucose and cellulose. Grafting of colloidal Ni nanoparticles proves to be the best preparation method. These catalysts quantitatively convert phenol and, upon optimization, afford 90% selectivity to the saturated hydrocarbon, cyclohexane, in hexadecane solvent under mild reaction conditions (473 K, 4 MPa  $\text{H}_2$ ).

Physicochemical characterization shows that the glucose- and cellulose-derived carbons exhibit drastically different textural properties, morphologies, and physicochemical properties. However, after sulfonation these carbon materials show similar activities in four cyclohexanol dehydration. This is attrib-



**Figure 9.** Product distributions on hydrodeoxygenation of phenol over: a)  $\text{Ni/C}_{\text{Zn-GI}}\text{-SO}_3\text{H}$ , and b) physically mixed  $\text{Ni/C}_{\text{Zn-GI}}\text{-SO}_3\text{H}$  and  $\text{C}_{\text{Zn-GI}}\text{-SO}_3\text{H}$  catalysts as a function of time. Conditions: phenol (1.0 g), hexadecane (60 mL), 473 K, 4 MPa  $\text{H}_2$ , stirring at 700 rpm, a)  $\text{Ni/C}_{\text{Zn-GI}}\text{-SO}_3\text{H}$  (10 wt %, 0.15 g), and b)  $\text{Ni/C}_{\text{Zn-GI}}\text{-SO}_3\text{H}$  (10 wt %, 0.15 g),  $\text{C}_{\text{Zn-GI}}\text{-SO}_3\text{H}$  (0.01 g).

uted to the similar concentrations of acidic functional groups (most importantly,  $-\text{SO}_3\text{H}$ ).

In contrast to be an efficient HDO catalyst in hexadecane, the current bifunctional formulations catalyse only ring hydrogenation of phenol without deoxygenation in the presence of water. In situ XAFS measurements demonstrate that the active metallic Ni phase in the  $\text{Ni/C-SO}_3\text{H}$  catalysts is stable in the aqueous phase under HDO conditions. Therefore, acid functions in the bifunctional  $\text{Ni/C-SO}_3\text{H}$  catalysts seem to be inhibited in the aqueous environments, in contrast to the metal-free carbon supports, which are able to dehydrate alcohols in both water and hexadecane.

In situ IR measurements used to follow the evolution of intermediate products over time show that the HDO of phenol on the  $\text{Ni/C-SO}_3\text{H}$  catalysts in hexadecane proceeds by a cascade of steps (ring hydrogenation, dehydration and hydrogenation) similar to those reported previously on noble metals. The rate-determining step is shown to be the acid-catalysed dehydration of cyclohexanol. Thus, adding  $\text{C-SO}_3\text{H}$  to the  $\text{Ni/C-}$



SO<sub>3</sub>H catalyst allowed the adjustment of the balance between acid and metal sites required to catalyse HDO optimally.

## Experimental Section

### Catalyst preparation

Carbon supports bearing SO<sub>3</sub>H groups carbon blacks were produced by pyrolysis of D-glucose or α-cellulose in N<sub>2</sub> flow (flow rate: 100 mL min<sup>-1</sup>) at 748 K with a heating rate of 5 K min<sup>-1</sup> for 15 h. The HS carbons were synthesized by impregnating the raw materials with an aqueous hydrochloric solution with enriched ZnCl<sub>2</sub> (75 wt% of the raw material). After 2 h stirring the acidic aqueous phase was removed by rotation evaporation, whereas the cellulosic suspension was filtered under vacuum. Before pyrolysis both ZnCl<sub>2</sub> impregnated raw materials were dried at 120 °C. LS and HS carbons were then washed with ultrapure water (363 K) and dried at 383 K for 24 h. In a Schlenk line, the resultant carbon material (5 g) was sulfonated with concentrated sulfuric acid (96 wt%, 150 mL) at 423 K for 15 h. After reaction, the black solid was filtered and then washed with ultrapure water (363 K) until the pH of the filtrate became neutral. Finally, it was dried in a convection oven at 383 K, overnight.

### Loading of Ni nanoparticles on C-SO<sub>3</sub>H support

The carbon-supported Ni catalysts were synthesized by three methods:

- Impregnation and thermal reduction with H<sub>2</sub>: Ni(NO<sub>3</sub>)<sub>2</sub>·6H<sub>2</sub>O was dissolved in methanol (30 mL), and the solution was slowly dropped onto C-SO<sub>3</sub>H support with stirring. After 1 h of stirring, the catalyst was dried at 373 K for 8 h, flushed with N<sub>2</sub> (flow rate) for 1 h and reduced under a H<sub>2</sub> flow (flow rate: 100 mL min<sup>-1</sup>) at 623 K for 3 h with a heating rate of 1 K min<sup>-1</sup>.
- Chemical reduction with ethylene glycol.<sup>[38]</sup> Ni(acac)<sub>3</sub> precursor and C-SO<sub>3</sub>H support were dispersed in ethylene glycol in a three-neck flask under vigorous stirring. The solution was heated to 513 K for 2 h with continuous stirring and refluxing. After that, the solution was cooled to ambient temperature and washed with absolute ethanol, and then sequentially filtered and dried under N<sub>2</sub> flow (flow rate: 100 mL min<sup>-1</sup>) for 8 h at ambient temperature.
- Grafting as-synthesized Ni nanoparticles reduced by borane triethylamine: a mixture of Ni(acac)<sub>3</sub> (2.57 g), oleylamine (150 mL) and oleic acid (3.2 mL) was loaded into a 250 mL two-neck Schlenk flask under N<sub>2</sub> flow and the mixture was stirred for 1 h at 383 K to remove oxygen and humidity. The blue Ni<sup>II</sup> solution was cooled to 363 K and the reducing agent triethylamine borane (2.5 mL) was quickly added. The resulting black mixture was stirred for 1 h and then cooled to ambient temperature. The black nanoparticles were washed with ethanol (300 mL), separated from the ethanol by centrifugation at 4000 rpm (1664 g) and redispersed in hexane (300 mL), in sequence. Finally, the Ni particles were grafted onto carbon support (2.5 g) by stirring the mixture for 3 days at ambient temperature and the solvent hexane was removed by rotary evaporation under vacuum.

### Catalyst characterization

#### Inductive coupled plasma-optical emission spectroscopy (ICP-OES)

The Ni contents on carbon supports were analysed by ICP-OES with a SpectroFlame Spectro Analytica Instrument FTMOA81A.

Before measurement, a calibration series of 0, 25, 50, 75, and 100 ppm Ni was prepared by diluting analytical standard 1000 ppm Ni (Fluka) in 0.5 M aqueous HNO<sub>3</sub> solution.

#### Specific surface area and porosity

Nitrogen sorption analysis was carried out at 77 K using a PMI automated sorptometer. BET surface areas and pore volumes were acquired from N<sub>2</sub> adsorption-desorption isotherms over a pressure range from 0.01 to 0.1 *p/p*<sub>0</sub>.

#### Boehm titration

Boehm titration was carried out to determine the concentration of –SO<sub>3</sub>H, –COOH, –OH groups on carbon materials. C-SO<sub>3</sub>H (0.5 g) was agitated with 50 mL of 0.05 M NaOH, NaHCO<sub>3</sub> and Na<sub>2</sub>CO<sub>3</sub> solutions in separate batches with continuous stirring for 24 h. Then, the solution was filtered and degassed with N<sub>2</sub> for 2 h. A 10 mL aliquot was taken from the NaOH and NaHCO<sub>3</sub> solution and acidified with 20 mL of 0.05 M HCl, whereas the aliquot of Na<sub>2</sub>CO<sub>3</sub> was acidified with 30 mL of 0.05 M HCl to ensure complete neutralization. The solutions were then back-titrated with 0.05 M NaOH to a potentiometric point of pH 7.0. For the back-titration method, the following equation was used to calculate the overall surface site concentration.<sup>[39,40]</sup>

$$n_{\text{surface}} = \frac{n_{\text{HCl}}}{n_{\text{B}}} [B]V_{\text{B}} - ([\text{HCl}]V_{\text{HCl}} - [\text{NaOH}]V_{\text{NaOH}}) \frac{V_{\text{B}}}{V_{\text{A}}}$$

where [B] and V<sub>B</sub> are the concentration and volume of the base mixed with the carbon, respectively, V<sub>A</sub> is the volume of aliquot taken from the V<sub>B</sub>, and [HCl] and V<sub>HCl</sub> are the concentration and volume of the acid added to the aliquot, respectively.

#### X-ray diffraction (XRD)

X-ray powder diffraction (XRD) was performed on Philips X'Pert Pro System equipped with a Cu<sub>Kα</sub> radiation source (40 kV, 45 mA) with 1.08° min<sup>-1</sup> in the 2θ range of 5–70°.

#### Transmission electron microscopy (TEM)

The TEM images were recorded on a JEM-2010 JEOL transmission microscope operated at 120 kV, and over 300 particles were counted for size calculation. Before TEM measurement, an ultrasonicated methanol suspension of the solid samples was dropped onto a Cu grid.

#### Scanning electron microscopy (SEM), energy dispersed X-ray analysis (EDX)

SEM was performed on a JEOL JSM 7500F, high-resolution scanning electron microscope with cold emission electron gun, operated at 1 kV. Sample preparation followed the same procedure as TEM. EDX was performed during SEM measurements with a JEOL JED-2300F energy dispersive X-ray analyser with dry SD detector.

#### Solid-state magic angle spinning nuclear magnetic resonance (solid MAS NMR)

The <sup>13</sup>C solid-state MAS NMR spectra were obtained on a Bruker AV500 spectrometer (B<sub>0</sub> = 11.7 T) at 125.76 MHz with a spinning rate of 10 kHz. For <sup>13</sup>C MAS NMR measurements the samples were fully hydrated before packing them into a 4 mm ZrO<sub>2</sub> rotor. The

35 000 scans were recorded by a recycle time of 4 ms. The excitation pulse had a length of 5 ms, with a relaxation delay between transients of 0.5 s. The chemical shifts are reported relative to an external standard of adamantane ( $\delta = 29.472$  ppm).

### Raman spectroscopy

Raman spectra were collected with a Renishaw Raman spectrometer 1000 equipped with a CCD detector using a 514 nm diode laser for excitation and Si(111) wafer as an external standard.

### Thermal gravimetric analysis (TGA)

The thermal gravimetric analysis was performed on a Setaram TG-DSC 111 thermo analyser connected to a high-vacuum system. About 30 mg of the carbon sample was placed in a quartz sample holder and the measurement was started at 273 K under vacuum ( $p < 10^{-4}$  mbar) with an incremental heating rate of  $1 \text{ K min}^{-1}$  to reach 1000 K. The  $\text{SO}_2$  release from the sample was measured in a Pfeiffer Vacuum PrismaPlus mass spectrometer.

### X-ray absorption spectroscopy

The near-edge structure (XANES) and extended X-ray absorption fine-structure (EXAFS) measurements were performed at the Pacific Northwest Consortium/X-ray Science Division (PNC/XSD) bending-magnet beamline at Sector 20 of the Advanced Photon Source (APS) at Argonne National Laboratory (ANL). The experiments were performed in transmission mode with a focused beam ( $0.7 \times 0.6$  mm) sending  $10^{10}$  photons through the sample with a harmonic rejection of 5.6 mrad and 8100 eV to decrease the effects of harmonics. An Ni foil was placed downstream of the sample cell, as a reference to calibrate the photon energy of each spectrum. A continuous series of Ni-K edge spectra were acquired throughout the entire reaction sequence using either 4 min ( $k = 12 \text{ \AA}^{-1}$ ) or 12 min ( $k = 18 \text{ \AA}^{-1}$ ) acquisition times. The quantitative analysis allowed the evaluation of bond lengths and Debye–Waller factors (structural disorder;  $\sigma^2$ ) up to 6 Å from the core Ni atom. The data were processed with the ATHENA program<sup>[41,42]</sup> and subsequently analysed with the ARTEMIS program.<sup>[43]</sup> The Fourier transform of the  $k$ -space EXAFS data [both real and imaginary parts of  $\chi(R)$ ] were fitted to the FEFF9 theoretical model.<sup>[44]</sup> Reference standards used in the analysis included bulk (fcc) NiO, bulk (hcp)  $\alpha$ -Ni(OH)<sub>2</sub>, and bulk (fcc) Ni. Their lattice parameters were obtained from the literature.<sup>[45,46]</sup>

In situ measurements were performed using the microreactor cell and procedures described by Chase et al.<sup>[35]</sup> with a few modifications. HiP® medium pressure Hastelloy® tees with an internal volume of 2 mL were used as reactor cells. Glassy-carbon discs, 0.75 mm thick by 3 mm in diameter, were used as windows. The discs were affixed to through-bore plugs which had been machined such that the distance between the windows was approximately 1 mm. Samples containing approximately 30 mg catalyst were pressed into a pellet, 0.4 mm thick by 3.5 mm in diameter, and held between the windows by a polyether ether ketone (PEEK) mesh ( $35 \mu\text{m}^2$ ). Typically, the reactor was charged with 0.9 mL of 0.56 M phenol solution and then purged with  $\text{H}_2$  at room temperature using five fill/purge cycles, then filled to a pressure of approximately 4.9 MPa. (In some experiments water or no liquid at all was used.) A spectrum was recorded and then cell was heated to 473 K while repeatedly recording spectra. The reaction conditions ( $T = 473 \text{ K}$ ,  $p_{\text{total}} \sim 5 \text{ MPa}$ ) were maintained for periods of up to 12 h during acquisition of the X-ray spectra. The liquid contents of the cell were removed after reaction and analysed by capillary gas

chromatography (Agilent 7890A GC equipped with HP-5MS 25 m  $0.25 \mu\text{m}$  i.d. column, coupled with Agilent 5975C MS).

### In situ IR spectroscopic study of phenol HDO

In situ IR spectra were recorded on the ReactIR 45 m device (Mettler Toledo) connected to the sentinel probe through the conduit K4. The sentinel probe is coupled to a Parr reactor (150 mL), where a diamond probe is used to collect the in situ IR spectra in the liquid phase (Figure S9 in the Supporting Information). Before measurement, the background was collected at reaction conditions (473 K, 3 MPa  $\text{H}_2$ ) with 1.0 g catalyst ( $\text{Ni/C}_{\text{GL-Zn}}\text{-SO}_3\text{H}$ ) dispersed in 50 mL hexadecane. Then the autoclave was loaded with the reactant phenol (5.0 g) and  $\text{H}_2$  (3 MPa) was charged at ambient temperature. The reactor was heated and the stirring was started once the temperature reached 463 K. The spectra were collected every 1 min for a total duration of 180 min, with  $8 \text{ cm}^{-1}$  spectral resolution and 256 scans per spectrum.

### Catalytic measurements

#### Cyclohexanol dehydration

In a typical experiment for cyclohexanol dehydration, a mixture of cyclohexanol (0.10 mol), hexadecane (60 mL), and  $\text{C-SO}_3\text{H}$  (0.5 g) was first charged into the reactor (Parr, Series 4843, 300 mL). After flushing the reactor with  $\text{H}_2$  three times, it was heated to 473 K at 5 MPa  $\text{H}_2$  while being stirred at 700 rpm; this was continued for 1 h at reaction temperature. After the reactor was cooled to room temperature, the  $\text{H}_2$  pressure was released and an aliquot of 2 mL was analysed by gas chromatography (GC, Shimadzu 2010) with a HP-5 capillary column ( $30 \text{ m} \times 250 \mu\text{m}$ ) and flame ionization detector (FID). Additionally, a gas chromatograph-mass spectrometer (GC-MS, Shimadzu QP 20105) was used to identify the organic compounds. The gas phase was determined by GC (HP 6890) equipped with a plot Q capillary column ( $30 \text{ m} \times 250 \mu\text{m}$ ) with thermal conductivity detector (TCD).

Phenol HDO was studied on  $\text{Ni/C-SO}_3\text{H}$  catalysts to evaluate the kinetic data in separated batches: a) phenol (6.4 mmol), hexadecane (60 mL),  $\text{Ni/C-SO}_3\text{H}$  (0.12 g), 473 K, 4 MPa  $\text{H}_2$ , and b) same conditions with physically admixed  $\text{C-SO}_3\text{H}$  (12, 25 and 60 mg). A typical reaction was performed in an autoclave batch reactor (Parr, Series 4843, 300 mL). After loading the reactant, catalyst, and hexadecane, the reactor was flushed three times with  $\text{H}_2$ . At reaction temperature,  $\text{H}_2$  was charged to a total pressure of 4.0 MPa and the mixture was allowed to react for 60, 120, 180, 240, 300 and 360 min while stirring at 700 rpm. After reaction, the work-up procedure was similar to that described above.

### Acknowledgements

This work was supported by the US Department of Energy (DOE), Office of Basic Energy Sciences (BES), Division of Chemical Sciences, Geosciences and Biosciences. Pacific Northwest National Laboratory is a multiprogram national laboratory operated for DOE by Battelle through Contract DE-AC05-76L01830. PNC/XSD facilities at the Advanced Photon Source, and research at these facilities, are supported by DOE/BES, the Canadian Light Source and its funding partners, the University of Washington, and the Advanced Photon Source. Use of the Advanced Photon Source, an Office of Science User Facility operated for the DOE Office of Science by Argonne National Lab-

oratory, was supported by the DOE under Contract No. DE-AC02-06CH11357.

**Keywords:** carbon support • IR spectroscopy • nanoparticles • phenol hydrodeoxygenation • X-ray absorption spectroscopy

- [1] T. P. Vispute, H. Zhang, A. Sanna, R. Xiao, G. W. Huber, *Science* **2010**, *330*, 1222–1227.
- [2] J. M. Thomas, *Angew. Chem. Int. Ed.* **1999**, *38*, 3588–3628; *Angew. Chem.* **1999**, *111*, 3800–3843.
- [3] C. O. Tuck, E. Pérez, I. T. Horváth, R. A. Sheldon, M. Poliakoff, *Science* **2012**, *337*, 695–699.
- [4] H. R. Bungay, *Science* **1982**, *218*, 643–646.
- [5] J. He, C. Zhao, J. A. Lercher, *J. Am. Chem. Soc.* **2012**, *134*, 20768–20775.
- [6] C. Zhao, J. He, A. A. Lemonidou, X. Li, J. A. Lercher, *J. Catal.* **2011**, *280*, 8–16.
- [7] C. Zhao, Y. Kou, A. A. Lemonidou, X. Li, J. A. Lercher, *Angew. Chem. Int. Ed.* **2009**, *48*, 3987–3990; *Angew. Chem.* **2009**, *121*, 4047–4050.
- [8] C. Zhao, Y. Kou, A. A. Lemonidou, X. Li, J. A. Lercher, *Chem. Commun.* **2010**, *46*, 412–414.
- [9] C. Zhao, J. A. Lercher, *Angew. Chem. Int. Ed.* **2012**, *51*, 5935–5940; *Angew. Chem.* **2012**, *124*, 6037–6042.
- [10] C. Zhao, S. Kasakov, J. He, J. A. Lercher, *J. Catal.* **2012**, *296*, 12–23.
- [11] C. Zhao, J. A. Lercher, *ChemCatChem* **2012**, *4*, 64–68.
- [12] C. Zhao, D. M. Camaioni, J. A. Lercher, *J. Catal.* **2012**, *288*, 92–103.
- [13] C. Zhao, Y. Yu, A. Jentys, J. A. Lercher, *Appl. Catal. B* **2013**, *132–133*, 282–292.
- [14] A. Gutierrez, R. K. Kaila, M. L. Honkela, R. Slioor, A. O. I. Krause, *Catal. Today* **2009**, *147*, 239–246.
- [15] J. Jiao, S. Seraphin, X. Wang, J. C. Withers, *J. Appl. Phys.* **1996**, *80*, 103–108.
- [16] P. Gorria, M. P. Fernández-García, M. Sevilla, J. A. Blanco, A. B. Fuertes, *Phys. Status Solidi RRL* **2009**, *3*, 4–6.
- [17] P. Gorria, M. Sevilla, J. A. Blanco, A. B. Fuertes, *Carbon* **2006**, *44*, 1954–1957.
- [18] A. B. Fuertes, P. Tartaj, *Chem. Mater.* **2006**, *18*, 1675.
- [19] A. B. Fuertes, P. Tartaj, *Small* **2007**, *3*, 275–279.
- [20] S. J. Tauster, S. C. Fung, R. T. K. Baker, J. A. Horsley, *Science* **1981**, *211*, 1121–1125.
- [21] M. Sevilla, A. B. Fuertes, *Carbon* **2009**, *47*, 2281–2289.
- [22] K. Nakajima, M. Okamura, J. N. Kondo, K. Domen, T. Tatsumi, S. Hayashi, M. Hara, *Chem. Mat.* **2008**, *21*, 186–193.
- [23] C. Falco, N. Baccile, M.-M. Titirici, *Green Chem.* **2011**, *13*, 3273–3281.
- [24] M. Kitano, K. Arai, A. Kodama, T. Kousaka, K. Nakajima, S. Hayashi, M. Hara, *Catal. Lett.* **2009**, *131*, 242–249.
- [25] K. Fukuhara, K. Nakajima, M. Kitano, H. Kato, S. Hayashi, M. Hara, *ChemSusChem* **2011**, *4*, 778–784.
- [26] M. Toda, A. Takagaki, M. Okamura, J. N. Kondo, S. Hayashi, K. Domen, M. Hara, *Nature* **2005**, *438*, 178.
- [27] X. Mo, E. Lotero, C. Lu, Y. Lin, J. G. Goodwin, *Catal. Lett.* **2008**, *123*, 1–6.
- [28] H. Yano, M. Kataoka, H. Yamashita, H. Uchida, M. Watanabe, *Langmuir* **2007**, *23*, 6438–6445.
- [29] Ö. Metin, V. Mazumder, S. Özkaz, S. Sun, *J. Am. Chem. Soc.* **2010**, *132*, 1468–1469.
- [30] M. Smisek, S. Cerny, *Active Carbon: Manufacture, Properties and Applications*, Elsevier, Amsterdam, **1970**.
- [31] N. Baccile, G. Laurent, F. Babonneau, F. Fayon, M.-M. Titirici, M. Antonietti, *J. Phys. Chem. C* **2009**, *113*, 9644–9654.
- [32] D. S. Knight, W. B. White, *J. Mater. Res.* **1989**, *4*, 385–393.
- [33] K. Nakajima, M. Hara, *ACS Catal.* **2012**, *2*, 1296–1304.
- [34] K. Nakajima, M. Hara, S. Hayashi, *J. Am. Ceram. Soc.* **2007**, *90*, 3725–3734.
- [35] Z. A. Chase, J. L. Fulton, D. M. Camaioni, D. Mei, M. Balasubramanian, V. Pham, C. Zhao, R. Weber, Y. Wang, J. A. Lercher, *J. Phys. Chem. C* **2013**, *117*, 17603–17612.
- [36] A. I. Frenkel, C. W. Hills, R. G. Nuzzo, *J. Phys. Chem. B* **2001**, *105*, 12689–12703.
- [37] W. Song, C. Zhao, J. A. Lercher, *Chem. Eur. J.* **2013**, *19*, 9833–9842.
- [38] J. W. Han, H. Lee, *Catal. Commun.* **2012**, *19*, 115–118.
- [39] S. L. Goertzen, K. D. Thériault, A. M. Oickle, A. C. Tarasuk, H. A. Andreas, *Carbon* **2010**, *48*, 1252–1261.
- [40] A. M. Oickle, S. L. Goertzen, K. R. Hopper, Y. O. Abdalla, H. A. Andreas, *Carbon* **2010**, *48*, 3313–3322.
- [41] B. Ravel, M. Newville, *J. Synchrotron Radiat.* **2005**, *12*, 537–541.
- [42] M. Newville, *J. Synchrotron Radiat.* **2001**, *8*, 322.
- [43] E. Bayram, J. C. Linehan, J. L. Fulton, J. A. S. Roberts, N. K. Szymczak, T. D. Smurthwaite, S. Ozkar, M. Balasubramanian, R. G. Finke, *J. Am. Chem. Soc.* **2011**, *133*, 18889–18902.
- [44] J. J. Rehr, J. J. Kas, F. D. Vila, M. P. Prange, K. Jorissen, *Phys. Chem. Chem. Phys.* **2010**, *12*, 5503–5513.
- [45] N. Smith, *J. Am. Chem. Soc.* **1936**, *58*, 173–179.
- [46] H. Bode, K. Dehmelt, J. Witte, *Electrochim. Acta* **1966**, *11*, 1079–1087.

Received: September 12, 2014

Published online on November 27, 2014